Indian Journal of Pure & Applied Physics
Vol. 63, May 2025, pp. 391-408
DOI: 10.56042/ijpap.v63i5.15087

The Influence of Filler Particle Size, Concentration and Distribution on Dielectric Properties of Epoxy Resin- Ceramic Composites Using Mixture Laws

L Chioukh*, H Khouni & N Bouzit

Laboratoire d'Instrumentation Scientifique LIS, Département d'Electronique, Faculté de Technologie, Université Ferhat Abbas Sétif 1, Sétif 19000, Algérie

Received:14 November 2024; accepted: 4 April 2025

Finite Element Method (FEM) simulations of the effective permittivity of several two-dimensional Epoxy Resin-Ceramic ellipsoid particle composites (RC) were performed in quasistatic limit. Using an algorithm developed, three distribution models (Normal, Log-normal, and Rayleigh) were applied to randomly generate a large number of particles. In order to explore the effect of particle morphology on the effective permittivity, an extensive study was conducted on three RC composites of different ceramic filler permittivity (ε_i =80, 400, and 3600). The results show the major impact of particle size, distribution, surface fraction, and permittivity ε_i on increasing the effective permittivity of composites. In addition, the permittivities obtained by FEM were compared with classical and modified theoretical models to determine the most suitable model. It was found that the modified Maxwell Garnett and Yamada models accurately predict the increase in permittivity as a function of surface fraction with an error rate of less than 0.2. The results of this research are essential for optimizing the performance of materials used for energy storage and harvesting, sensors, and various electrical and electronic devices before their design.

Keywords: Ceramic, Composite, Epoxy resin, Distribution models, Permittivity, Finite element method, Mixing laws

1 Introduction

The growing demand for advanced technology has led to the emergence of composite materials in various industries due to their unique properties that conventional materials cannot provide[1,2]. These materials are typically composed of two or more distinct constituent materials that can be physically or chemically combined to achieve specific properties[3]. The constituent materials are arranged in a distributed phase, with the matrix often comprising a ceramic material embedding a filler phase[4-6]. In order to design customized materials that meet specific requirements in terms of electromagnetic properties, several efforts have been made to understand the influence of constituent phases, their proportions and particle morphology on the dielectric behavior of the composite material[7-10]. Over the last four decades, several numerical simulation and modeling techniques have been developed to understand and predict the relationships between the structure and behavior of composite materials[11,12]. Today, these techniques have become a third research path between theory and experiment, where they can address most of the open physical problems, thus providing a deep understanding of the behavior of materials at the microscopic and macroscopic scales. Using these numerical methods, researchers can explore in detail the impact of factors such as particle shape, size and distribution on the electromagnetic properties of dielectric composites[13,14]. One of the most practical and powerful numerical methods used in simulation to predict the dielectric behavior of composites is the finite element method (FEM), which is widely documented in the literature[15-19]. This technique is used to solve complex technical and scientific problems that involve solving partial differential equations (PDEs).

To validate numerical models and improve our understanding of the behavior of composite materials, it is essential to compare the predicted behavior with theoretical models, also called "mixing laws". In most of these models, the study of composite properties has been based on a quasistatic approach, where variations of the electromagnetic field are slow compared to the physical phenomena of the material,

*Corresponding author: (E-mail: labiba.chioukh@univ-setif.dz; chioukh612@gmail.com)

which allows a simplified analysis of the interaction between the field and the composite material and to understand the link between microscopic and macroscopic properties by identifying the effective permittivity of heterostructures. Researchers have proposed several theoretical formulas, and each has its own set of assumptions and restrictions that determine its applicability to specific types of composite materials[20-24].

Our goals for the current study are twofold. Initially, to look at the effects of ceramic particle size, permittivity, concentration, and distribution on the dielectric behavior of binary composite materials composed of epoxy resin and ceramic particles (RC). Second, we aim to further study the dielectric behavior in RC composites by exceeding the number of particles studied in previous works[25-28]. To achieve this, the Finite Element Method was used to simulate several two-dimensional RC composite samples. FEM is recognized as a robust tool for composite characterization. However, its major drawback lies in its high requirements in computing resources and memory space. For this reason, we opted for the two-dimensional (2D) electromagnetic analysis approach. Not only does it significantly reduce the computational requirements, but it also helps us achieve our second objective. Using a newly designed algorithm, several probability distribution models were applied (Normal, Log-normal, and Rayleigh) to randomly simulate ellipsoid particles. By varying its mean and standard deviation parameters, we have effectively succeeded in studying and analyzing the impact of particle size and distribution on the effective permittivity of composites. In addition, the simulation results obtained were compared with several theoretical "mixing law" models. By applying this comparison, we aimed to identify the most suitable one capable of accurately representing the concentration and size of the particles. The knowledge gained from this research can offer valuable guidance for optimizing the design and performance of these materials, enabling their tailored applications in various industries, such as electronics, telecommunications, and energy storage systems.

2 Work Methodology

2.1 Simulation Methodology

2.1.1 Model Structure and Computational Details

Our paper focuses specifically on the study of the effective permittivity of random and lossless dielectric composite materials in the quasi-static state. The quasi-static regime is determined when the temporal variations of the electromagnetic field are negligible compared to the spatial variations. This condition is valid when the wavelength of the incident wave is much larger than the typical size of the inhomogeneities presented in the material.

The study consisted in simulating several samples with different permittivities, sizes, concentration, and distribution of ellipsoidal particles. This was achieved by doing a numerical modeling using COMSOL Multiphysics®[29] software version 5.6 which integrates all the functions of MATLAB software containing the parameters of each particle distributed in the epoxy resin polymer matrix. This software uses the finite element method to develop and solve the quasistatic models. A thorough description of this method is available in the literature[15, 30,31].

Figure 1 shows the geometry of the unit cell of the composite under study. This cell has dimensions equivalent to those of the rectangular WR-90

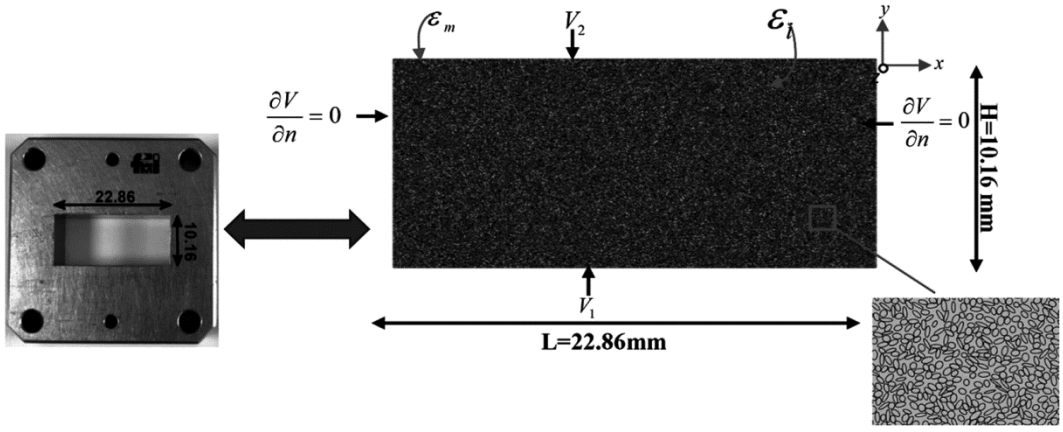

Fig. 1 — (a) Rectangular waveguide WR-90, and (b) Unit cell of the composite material studied and boundary conditions

waveguide (0.9 in [22.86 mm] x 0.4 in [10.16 mm]). Our two-dimensional structure of the binary composite consists of an epoxy resin host matrix of permittivity $\varepsilon_m = 2$, and ellipsoidal ceramic particles randomly distributed without overlap in the matrix. In order to determine the evolution of the effective permittivity as a function of the surface fraction, the permittivity ε_i , and the particle sizes, the finite element method was used.

Consider the unit cell in Fig. 1 as a capacitor model. It is composed of two opposite faces with a area A and a height H between them. These faces are subject to a potential difference

(V_1-V_2). The periodic boundary conditions $\partial V / \partial n = 0$ are applied to the planes parallel to the direction (Oy). To calculate the effective permittivity, the FEM uses a finely discretized mesh of the spatial domain, where it divides the rectangular geometry into smaller triangular elements (Fig. 2).

This meshing strategy facilitates the precise calculation of the spatial distribution of the potential (Fig. 3) inside this geometry, which is devoid of free charges or currents, via the resolution of Laplace's equation:

$$\vec{\nabla}\cdot(\varepsilon_0\varepsilon(r)\vec{\nabla}V)=0 \qquad \ldots (1)$$

With $\varepsilon(r)$ and V representing respectively the local relative permittivity and the spatial distribution of the potential in the cell, where the free charge density is zero, and $\varepsilon_0 = 8.85\times10^{-12}\left[F/m\right]$ as the permittivity of vacuum, the electrostatic energy W can be expressed in terms of the partial derivatives of V over the entire surface of the unit cell.

$$W=\frac{1}{2}\varepsilon_0\iint_s\varepsilon(x,y)\left[\left(\frac{\partial V}{\partial x}\right)^2+\left(\frac{\partial V}{\partial y}\right)^2\right]dxdy \qquad \ldots (2)$$

By imposing periodic boundary conditions $\partial V / \partial n = 0$ on the planes parallel to the direction (Oy). the effective permittivity is obtained by evaluating the energy stored in the capacitor:

$$W=\frac{1}{2}\varepsilon_0\varepsilon_{eff}\frac{A}{H}(V_1-V_2)^2 \qquad \ldots (3)$$

2.1.2 Calculation Algorithm

To determine the parameters of the ellipses, we created a MATLAB code that integrates a computational algorithm. The main objective of the algorithm is to generate a non-overlap random distribution of ceramic particles in the epoxy resin matrix. To achieve this, the algorithm follows two

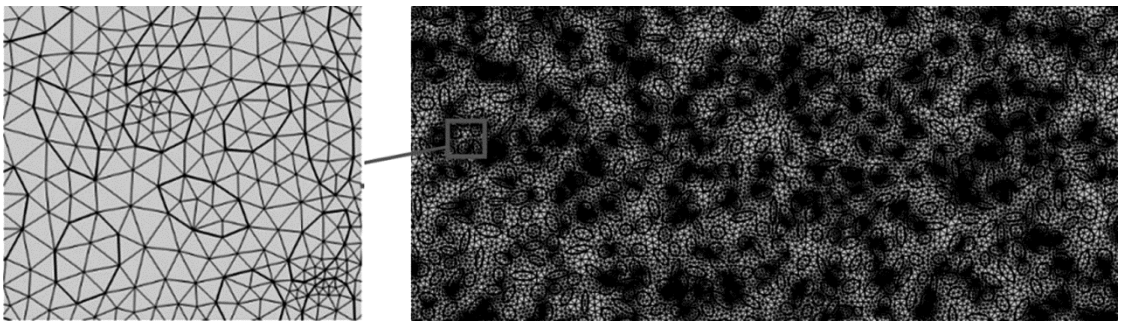

Fig. 2 — Mesh Representation of the unit cell

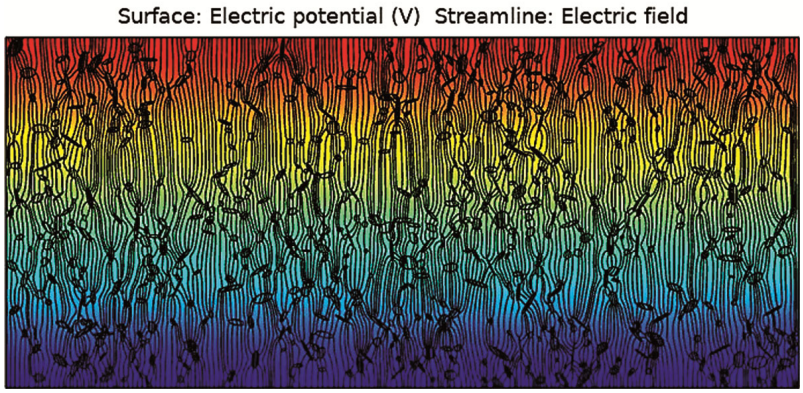

Fig. 3 — Spatial distribution of electric potential and electric field

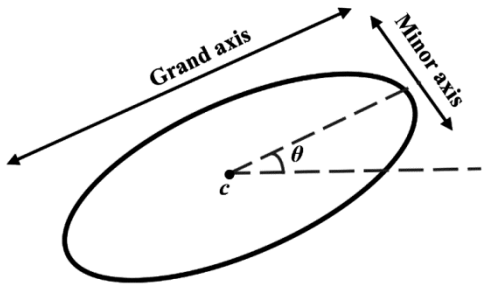

Fig. 4 — Illustration of the shape characteristics of an ellipse. The aspect ratio was calculated by dividing the grand axis by the minor axis

main procedures: particle surface area distribution and particle location determination. Here we present the outline of the developed generation algorithm.

a. Particle Surface Area Distribution Procedure

The algorithm takes several input parameters, including the total particle surface fraction, mean value of particles surface area (μ), standard deviation of particles (σ), minimum particle ratio (r_{min}), maximum particle ratio (r_{max}), minimum (x_{min}) and maximum (x_{max}) grand axis of ellipsoidal particles as shown in Fig. 4.

The particle size distribution procedure begins by generating particles one by one. Each particle is assigned a random ratio (r) within the specified range (r_{min} to r_{max}). This randomness influences the distribution of particle sizes within the polymer matrix.

b. Particle Location Determination Procedure

The procedure focuses on assigning positions to the generated particles within the polymer matrix. It calculates the x parameter, which characterizes particle location (c), based on the particle ratio and random values. The calculated (x) value must fall within the range defined by (x_{min}) and (x_{max}).

c. Intersection Avoidance

To ensure that the particles do not overlap, the algorithm checks whether the sum of the radii of the two ellipses is less than the distance between their centers (See Fig. 5). Mathematically this can be expressed by the equation 4. This check consists of solving a system of mathematical equations presented in[32]. If an intersection is detected, indicating particle overlap, the algorithm iteratively repositions the particles until no intersection occurs. The maximum number of iterations ($iter_{max}$) prevents the algorithm from getting stuck in infinite loops.

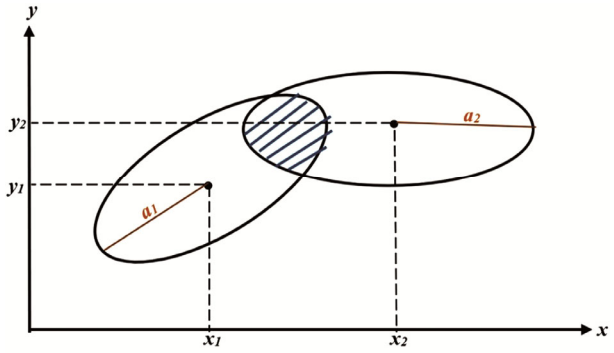

Fig. 5 — Illustration of two ellipses overlap

$$\sqrt{(x_2 - x_1)^2 + (y_2 - y_1)^2} \geq a_1 + a_2 \quad \ldots (4)$$

d. Surface Fraction Calculation

The algorithm calculates the surface fraction of the particles within the polymer matrix. This calculation is based on the areas of the ellipses and their corresponding particle ratios.

e. The particle generation and location determination steps continue until a specific condition is met, such as generating a desired number of particles or reaching a maximum iteration limit.

f. The resulting particle locations (c), grand axes (gx), small axes (sx), and surface fraction (S) are obtained as output.

To integrate the parameters of the ellipses obtained in the unit cell, we establish a connection between the MATLAB software and COMSOL using LiveLink[33]. This integration allows us to use the Finite element method available in COMSOL to extract the effective permittivity of the composite samples. It is noteworthy that this simulation may be time-consuming, particularly for distributions with a high concentration of particles.

2.2 Empirical Models using for Prediction of Dielectric Permittivity

Many theoretical investigations have been carried out to understand the dielectric behavior of composites[34], considering the dielectric constant of the matrix and load, their volume fraction, and their interactions. However, basic models have limitations as they overlook the impact of inclusion particle size and shape, as well as the interface between the matrix and filler. To overcome these constraints, complex models have been developed, but their equations do not entirely align with experimental results.

In this study, we divided the theoretical models into two groups. and conducted a thorough comparison and critical analysis to understand the

dielectric behavior of composites. Our focus was on evaluating the main parameters considered by each model and determining which is more suitable for considering filler concentration, particle distribution, and particle size. The first group is the original empirical models which assume that the composite consists of spherically shaped inclusions that are dispersed in a continuous matrix, without taking into account any factors such as depolarization, shape, and distribution. In contrast to the second group that presents the modified laws, where they take into account these factors.

The equations below all use v to represent volume fraction and ε to represent dielectric constant. The subscripts "m" and "i " distinguish between the matrix and inclusions, respectively.

2.2.1 Original Empirical Models

Dielectric permittivity studies of heterogeneous materials date back to the last century and were initially focused on mixtures with asymmetric geometry. Clausius and Mossotti first computed the permittivity of a group of molecules in a vacuum, which was later extended by Maxwell-Garnett [35] to include inclusions of varying sizes in an isotropic and homogeneous medium.

$$\varepsilon = \varepsilon_m + 3v\varepsilon_m \frac{\varepsilon_i - \varepsilon_m}{\varepsilon_i + 2\varepsilon_m - v(\varepsilon_i - \varepsilon_m)} \quad \ldots (5)$$

In[36], Lichtenecker proposed a simple model for the scenario where spherical dielectric inclusions are present in an isotropic dielectric medium. This model enables easy computation and quick estimation of the effective permittivity.

$$\ln(\varepsilon) = (1-v)\ln(\varepsilon_m) + v\ln(\varepsilon_i) \quad \ldots (6)$$

A few years later, Bruggeman[37] proposed an alternative to the Maxwell-Garnett model to address the problem of uncertainty that arises with high concentrations of inclusions. Unlike the Maxwell-Garnett model, the Bruggeman model does not consider the existence of a host material. Instead, it assumes that the particles of any component of a simple material are embedded in an effective medium with a permittivity that is equal to the permittivity of the mixture being studied (ε).

$$\varepsilon = \varepsilon_i \left[\frac{3\varepsilon_m + 2v(\varepsilon_i - \varepsilon_m)}{3\varepsilon_i - v(\varepsilon_i - \varepsilon_m)} \right] \quad \ldots (7)$$

Assuming an almost random distribution of spherical inclusions within a matrix and accounting for the interactions between these particles, an equation was derived by Looyenga[38] .

$$(\varepsilon)^{1/3} = (\varepsilon_i)^{1/3} v + (\varepsilon_m)^{1/3}(1-v) \quad \ldots (8)$$

2.2.2 Modified Empirical Models

These models extend the effects considered in group 1 by incorporating shape, orientation, and distribution information of the inclusions, often assumed as ellipsoids. Equations in these models include depolarization factors (A), shape parameters (n) to account for the additional information.

The modified version of the Maxwell-Garnett[39] formula is represented by Eq. 9, which considers the depolarization factor of the inclusions (where $0 < A < 1$). For a circular geometry, the value of A is equal to 1/2.

$$\varepsilon = \varepsilon_m \left(1 + \frac{v\left[\varepsilon_i / \varepsilon_m - 1\right]}{1 + A(1-v)\left[(\varepsilon_i / \varepsilon_m) - 1\right]}\right) \quad \ldots (9)$$

The Bruggeman effective medium approximation formula has a modified[39] version that can be used to estimate the effective dielectric constant of a composite material made of two different constituents.

$$\varepsilon = 1/2(1-A')\left[1\text{-}A'\left(1+\left(\varepsilon_i/\varepsilon_m\right)\right)+v\left(\varepsilon_i/\varepsilon_m\text{-}1\right) \pm \left(\left(1\text{-}A'\left(1+(\varepsilon_i/\varepsilon_m)\right)+(1\text{-}v)\left((\varepsilon_i/\varepsilon_m)\text{-}1\right)\right)^2 + 4A'(1\text{-}A')(\varepsilon_i/\varepsilon_m)\right)^{1/2}\right] \quad \ldots (10)$$

In[40], Bergman developed a theoretical model to calculate the effective dielectric properties of composite materials containing ellipsoidal inclusions. The Bergman model takes into account the depolarization factor of the inclusions and is based on solving the electric field inside and around the inclusions.

$$\varepsilon = \varepsilon_m + v\varepsilon_i \frac{\varepsilon_m - \varepsilon_i}{\varepsilon_i + A''(\varepsilon_m - \varepsilon_i)} \quad \ldots (11)$$

Yamada *et al*[41]. obtained the below equation for a random distribution of ellipsoidal particles in a continuous matrix, where the shape of the particles is represented by a shape parameter, denoted as n.

$$\varepsilon = \varepsilon_m \left[1 + \frac{nv(\varepsilon_i - \varepsilon_m)}{n\varepsilon_m + (1-v)(\varepsilon_i - \varepsilon_m)}\right] \quad \ldots (12)$$

3 Results and Discussion

Dielectric composites, which generally combine ceramic particles with a polymer matrix, offer a remarkable synergy between the properties of the two materials: the flexibility and lightness of the polymer, combined with the high permittivity and low dielectric losses of ceramics. However, the performance of these composites is not limited to the dielectric constant of the ceramic particles. Aspects such as the shape, size and distribution of particles in the polymer matrix, as well as their volume fraction, also play a significant role in the overall performance of the material. In this section, we explore the impact of these parameters on the overall permittivity through detailed simulations, allowing an in-depth analysis of the influence of microstructure on dielectric properties. Furthermore, we examine how mixing laws can be used to model the dielectric constant, highlighting the relevance and accuracy of these approaches in predicting the electromagnetic behavior of composites. By integrating these two aspects, our study provides essential insights for the design and optimization of advanced dielectric composites, paving the way for further advancements in various fields of electronics and telecommunications.

3.1 Dielectric Constant Sweep

In our study, we employed epoxy resin with a constant permittivity of (ε_m= 2) as a matrix to bind the charged ceramic particles. We analyzed the dielectric permittivity of three epoxy resin/ceramic (RC) composites with ceramic permittivities (ε_i) of 80, 400, and 3600, respectively. For each composite, we performed simulations on several samples, varying the surface fraction (S) of ellipsoidal particles included in the matrix from 0.05 (5%) to about 0.4 (40%). Each composite was modeled according to three random distributions of ceramic particles: normal (N), log-normal (LN), and Rayleigh (R). For each distribution, we examined three cases of different particle sizes. This approach allowed us to study the impact of the permittivity of the ceramic particles, their concentration, their size and their distribution on the overall permittivity of the composite.

3.1.1 Normal Distribution (N)

The normal distribution (N), also called the Gaussian distribution, is widely used to model various physical systems due to its ease of use and flexibility. In our case study, we apply this distribution to the surface area of ellipsoid-shaped particles present in an epoxy polymer matrix. This approach allows us to statistically characterize the distribution of areas within the matrix, which results in a distinctive bell-shaped curve in our curves (Figs. 6-8 (a)).

Table 1 lists the designation and composition of 3 sets of simulated RC samples. each series represents a distinct case of particle sizes that follow the normal distribution N-(RC), which is defined by the mean area μ and the standard deviation σ values

Figure 6 (a) shows the normal distribution of the simulated samples for case N-$(RC)_1$, giving us an idea of how the particle sizes are spread out. The average particle size is 0.1 mm², with a small standard deviation of 0.005 mm², meaning most of the particles are quite similar in size.

Figure 6 (b-c) present 2D COMSOL simulations of two different samples, helping to visualize how the particles are distributed in the material. Fig. 6 (b) represents the first sample, where the particle surface fraction (S) is 0.05, so the particles are more spaced

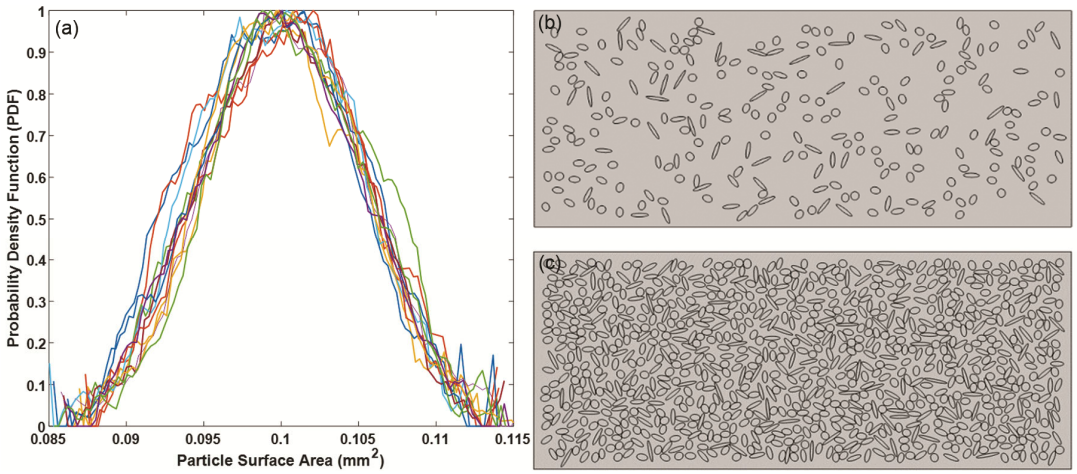

Fig. 6 — N-$(RC)_1$**:** (a) Normal distribution of all samples, (b) Sample N° 1 (S=0.059), (c) Sample N° 12 (S=0.399)

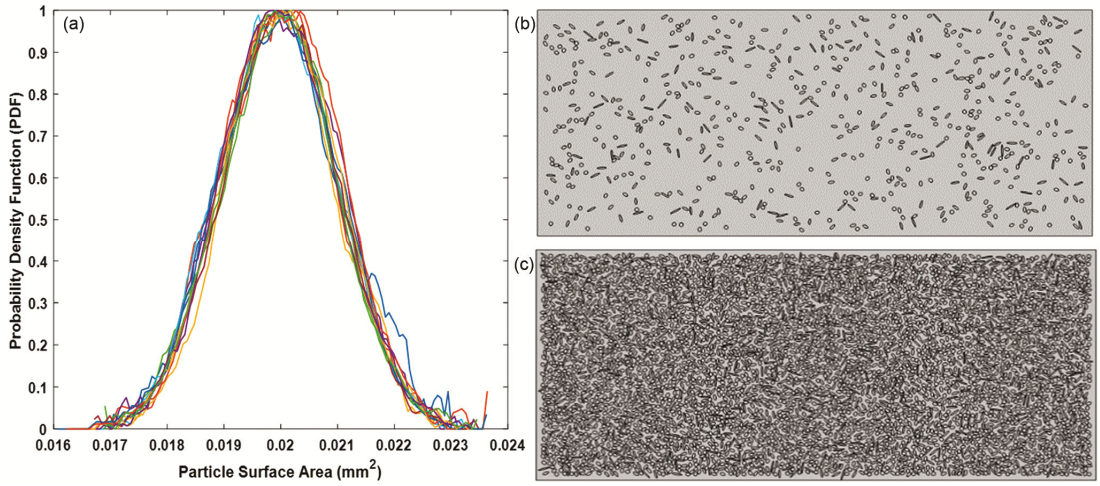

Fig. 7 — N-$(RC)_2$: (a) Normal distribution of the samples, (b) Sample N° 1 (S=0.052), **(c)** Sample N° 12 (S=0.395).

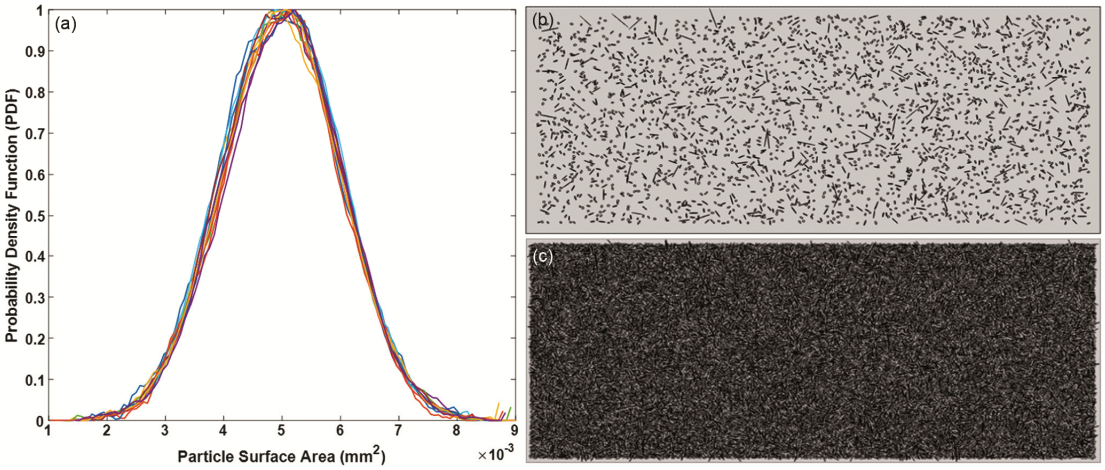

Fig. 8 — N-$(RC)_3$: (a) Normal distribution of the samples, (b) Sample N° 1(S=0.052), **(c)** Sample N° 11 (S=0.392)

Table 1 — Characteristics of three series of RC composites simulated using the Normal Distribution (N)

	N-$(RC)_1$		**N-$(RC)_2$**		**N-$(RC)_3$**	
	μ=0.1 mm², σ=0.005 mm²		μ=0.02 mm², σ=0.001 mm²		μ=0.005 mm², σ= 0.001 mm²	
***N°* Samples**	***N^0 particles***	***S***	***N^0 particles***	***S***	***N^0 particles***	***S***
1	250	0.059	600	0.052	2600	0.052
2	300	0.109	1000	0.087	4400	0.087
3	350	0.131	1400	0.112	6200	0.122
4	400	0.163	1800	0.147	7995	0.157
5	450	0.194	2200	0.172	9795	0.192
6	500	0.226	2600	0.207	11589	0.227
7	550	0.259	3000	0.232	13361	0.262
8	600	0.281	3400	0.267	15154	0.297
9	650	0.311	3800	0.292	16841	0.332
10	700	0.344	4200	0.327	18528	0.367
11	750	0.375	4600	0.357	20215	0.392
12	800	0.399	5000	0.395		

out. On the other hand, Fig. 6 (c) corresponds to the last sample, with S = 0.39, where the particles are much denser. Even though this sample has a higher fraction of particles, their relatively large size means there aren't that many overall, with only 800 particles.

Figure 7 illustrates the distribution of N-$(RC)_2$ and presents 2D models of the first and last samples. A key difference compared to N-$(RC)_1$ is the smaller particle size of 0.02 mm², which significantly impacts the overall microstructure. Since the particles are much smaller, there is a higher number of ellipsoidal inclusions in the composite, as clearly depicted in Fig. 7 (b–c).

For instance, when considering the last sample from Table 1 with S = 0.39, we observe a remarkable increase in particle density, with approximately 5,000 particles embedded within the epoxy matrix. This sharp contrast with N-$(RC)_1$ (which had only 800 particles for the same S value) highlights the influence of particle size on dispersion and composite microstructure. The higher number of inclusions suggests a greater interfacial area between the particles and the surrounding matrix, which may lead to enhanced dielectric and mechanical properties, depending on particle-matrix interactions.

For the N-$(RC)_3$ case, interesting illustrations have been shown in Fig. 8. It is notable that the distribution of particles in this case has a lower mean (μ=0.005 mm^2) with a large standard deviation (σ=0.001mm^2), which results in a large number particles of various sizes. For the same case where S=0.39, there are 20215 inclusions.

Figure 9 represents the evolution of the effective permittivity depending on the surface fraction of the three series of simulated composite samples (N-$(RC)_1$, N-$(RC)_2$, and N-$(RC)_3$) for three cases of permittivity of ellipsoid particles ε_i= 80, 400 and 3600.

It is observed that the distribution of N-$(RC)_3$ particles gives a better permittivity compared to N-$(RC)_2$ and N-$(RC)_1$ in all cases of particle permittivity. It is likely that this is due to the diversity of particle sizes in this case, where the standard deviation is larger compared to the mean. This size diversity could lead to greater variability in the dielectric properties of the particles, which could help improve the overall permittivity of the composite. In addition, the number of inclusions is also large, which could enhance the interactions between the matrix and the filler. These matrix-filler interactions, resulting from a wider distribution of particles in the matrix, could play a crucial role in improving the dielectric properties of the composite material.

We also notice, for the three cases of permittivity of ceramic particles, When the surface fraction is low (S <0.1), indicating a low concentration of inclusions, minimal fluctuations in the permittivity values are observed, this is due to the minimum interaction between particles within the composite. These charge-matrix interactions become more important as S increases, producing a higher effective permittivity. This increase in dielectric permittivity indicates the same effect of titanates compared to that obtained in previous works[3,4,6,42].

On the other hand, it is evident that the ceramic charge permittivity has a direct impact on the electromagnetic interactions between the charge and the matrix in the composite material. When the permittivity of the ceramic is very high than the permittivity of the matrix (case of 400 and 3600), this means that the particles interact more strongly with the matrix, which can lead to a greater increase in the effective permittivity of the composite material. Let us take the example of sample N° 12 in Table 1 for case N-$(RC)_3$: at a surface fraction (S) of 0.39, the effective permittivity of the material varies. For a permittivity (ε_i) of 80, the effective permittivity value is measured at 6.3. This value increases to 7.4 when the permittivity is 400, then reaches 8 for a permittivity of 3600.

3.1.2 Log-Normal Distribution (LN)

A Log-normal distribution is a statistical distribution of logarithmic values derived from an associated

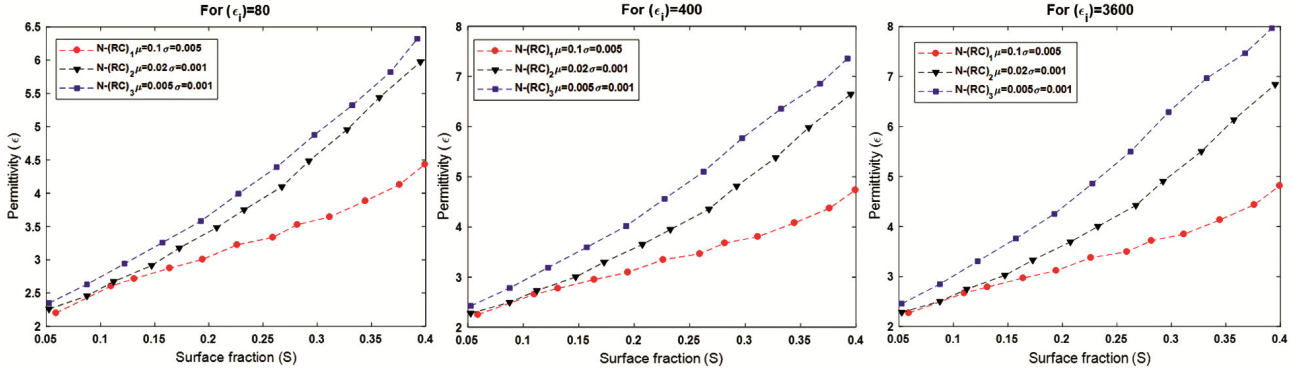

Fig. 9 — Evolution of the effective permittivity as a function of surface fraction for N-(RC) composites

Table 2 — Characteristics of three series of RC composites simulated using the Log-normal Distribution (LN)

	LN-(RC)$_1$		**LN-(RC)$_2$**		**LN-(RC)$_3$**	
	μ=0.1 mm^2 σ=0.15 mm^2		μ=0.03 mm^2 σ=0.02 mm^2		μ=0.01 mm^2 $\sigma = 0.01$ mm^2	
***N°* Samples**	***N^0 particles***	***S***	***N^0 particles***	***S***	***N^0 particles***	***S***
1	144	0.054	348	0.056	996	0.050
2	224	0.091	628	0.093	1688	0.090
3	310	0.132	900	0.133	2363	0.119
4	385	0.163	1450	0.171	3018	0.156
5	445	0.218	1700	0.212	3668	0.194
6	528	0.231	1955	0.239	4306	0.229
7	603	0.255	2440	0.259	4914	0.259
8	644	0.286	2635	0.288	5485	0.297
9	725	0.305	2824	0.306	6036	0.315
10	775	0.322	3150	0.326	6610	0.331
11	812	0.342	3307	0.345	7022	0.348
12	850	0.367	3403	0.365	7447	0.379
13	930	0.386	3518	0.373	7507	0.382
14	997	0.399	3661	0.398	7914	0.394

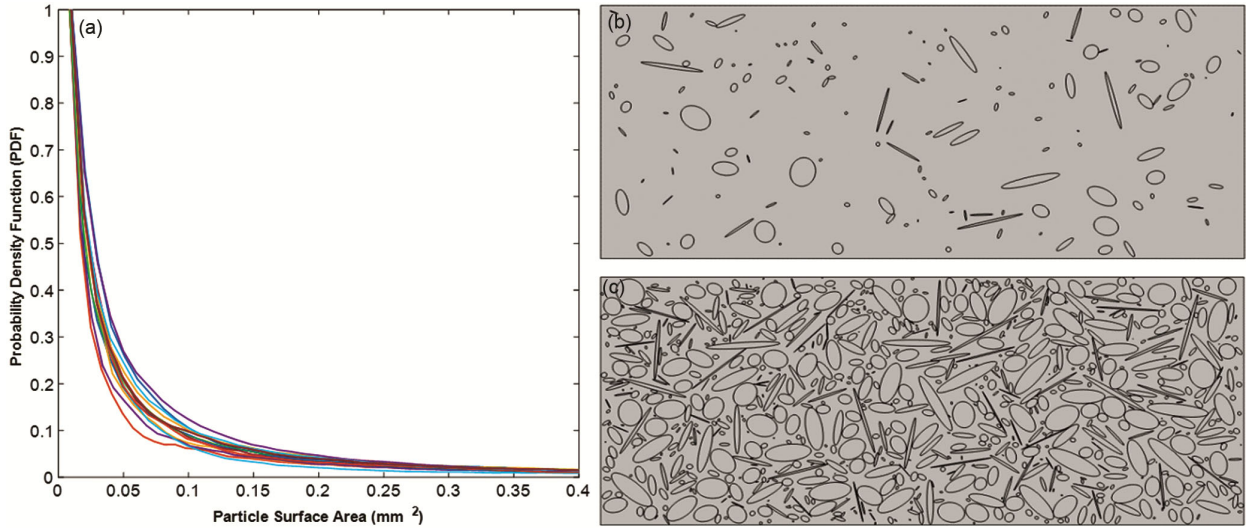

Fig. 10 — LN-(RC)$_1$: (a) Log-normal distribution of the samples, (b) Sample N° 1 (S=0.054), (c) Sample N° 14 (S=0.399)

normal distribution. The use of this distribution is appropriate for modeling a wide variety of particle sizes due to its skewed nature, characterized by a long tail to the right (see Figs. 10-12 (a)).

Table 2 shows the simulation results obtained by applying log-normal modeling to three distinct series (LN-(RC)$_1$, LN-(RC)$_2$, and LN-(RC)$_3$).

According to the three series illustrated in Figs. 10-12, we observed that there is a great variety in the sizes of the particles. This observation can be explained by the nature of this distribution on the one hand with the high value of σ on the other hand.

The particle distribution for the LN-(RC)$_1$ sample series is shown in Fig. 10 (a). A visualization of the particle distribution for sample N° 1 and 14, performed under COMSOL, is shown in Fig. 10 (b-c), respectively. Significant variability in particle sizes was observed given that standard deviation is large (σ= 0.15 mm^2) with a high mean surface area (μ = 0.1 mm^2). This translates into a relatively low number of inclusions. For example, in the last sample visualized in Fig 10.c, for a concentration of S=0.39, only 997 particles are present.

In LN-(RC)$_2$ and LN-(RC)$_3$, on the other hand, the number of particles increases as μ decreases. However, in this distribution, we encountered difficulties in the simulation of inclusions for lower standard deviation (σ) values, in contrast to the case of the normal distribution. The characteristics of this distribution can make the simulation more complex,

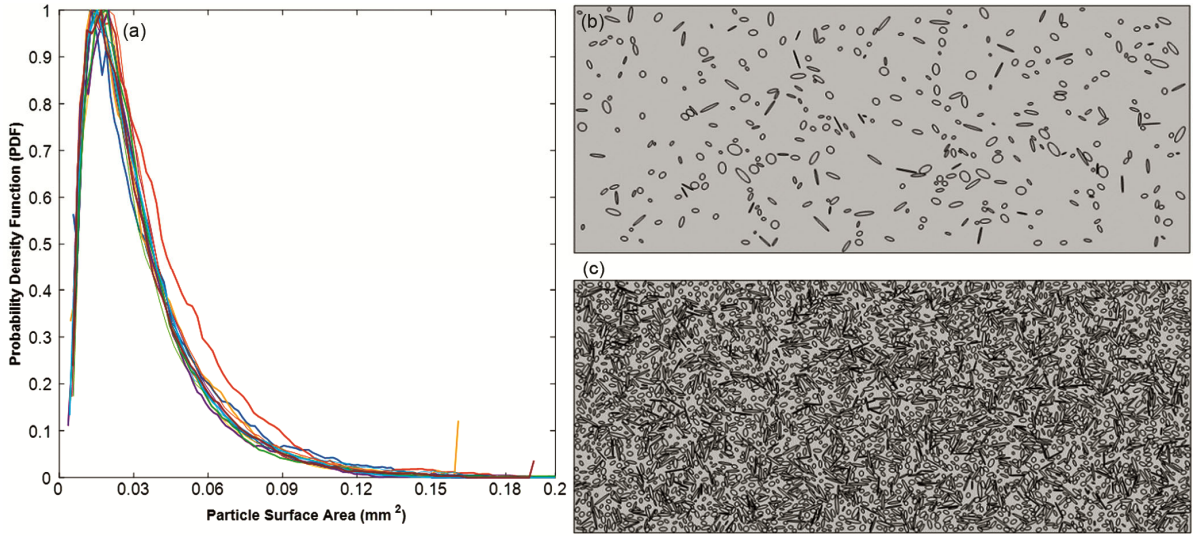

Fig. 11 — LN-$(RC)_2$: (a) Log-normal distribution of the samples, (b) Sample N° 1 (S=0.056), (c) Sample N° 14 (S=0.398)

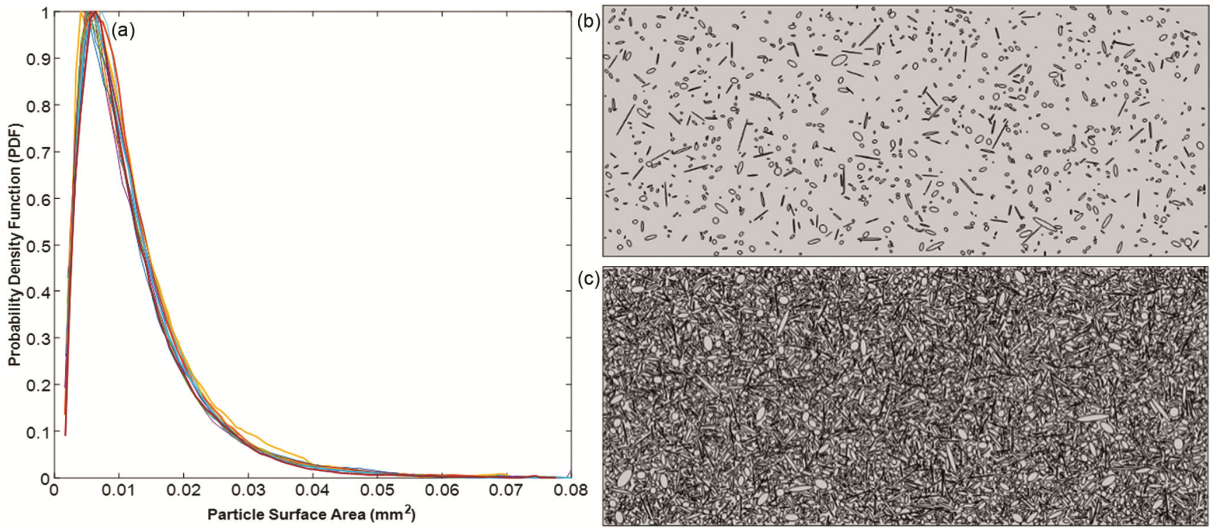

Fig. 12 -— LN-$(RC)_3$: (a) Log-normal distribution of the samples, (b) Sample N° 1 (S=0.50), (c) Sample N° 14 (S=0.394)

as the algorithm must guarantee an appropriate distribution of particles in the matrix without overlap, while taking into account the skewed nature and narrow range of the log-normal distribution.

The permittivity values found for the different series of simulated samples as a function of the surface fraction S when ε_i = 80, 400, and 3600, respectively, are shown in Fig. 13.

The graphs show that permittivity increases with increasing particle surface fraction (S). However, the permittivity (ε) found for the three distribution cases LN-$(RC)_1$, LN-$(RC)_2$, and LN-$(RC)_3$ is relatively close when the permittivity of the ceramic particles is relatively low (ε_i= 80). This behavior can be explained by two points: on the one hand, a ceramic particle permittivity of 80, which is not significantly higher than that of the epoxy matrix (ε_m=2), leads to a weaker polarization effect. On the other hand, particle size has a minimal impact on the overall permittivity of the composite, as they all interact in the same way with the weak polarization effect. In contrast, when the ceramic permittivity is significantly higher (400 and 3600), the inclusions exert a stronger influence on the effective permittivity of the composite. The large contrast between the matrix and particles permittivities leads to a stronger polarization effect, and the size of the particles becomes a more critical factor.

It is remarkable that LN- RC_3 gives a better permittivity than LN-RC_1 and LN-RC_2 for ε_i = 400 and ε_i = 3600, This is attributed to two parameters: a low mean (μ=0.01 mm2) associated with a large standard deviation (σ=0.01), indicating a large

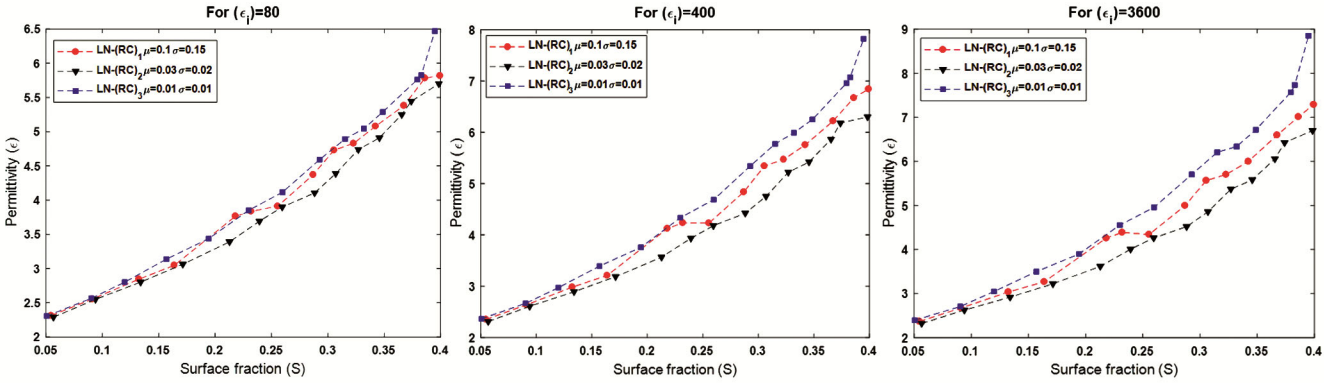

Fig. 13 — Evolution of the effective permittivity as a function of surface fraction for LN-(RC) composites

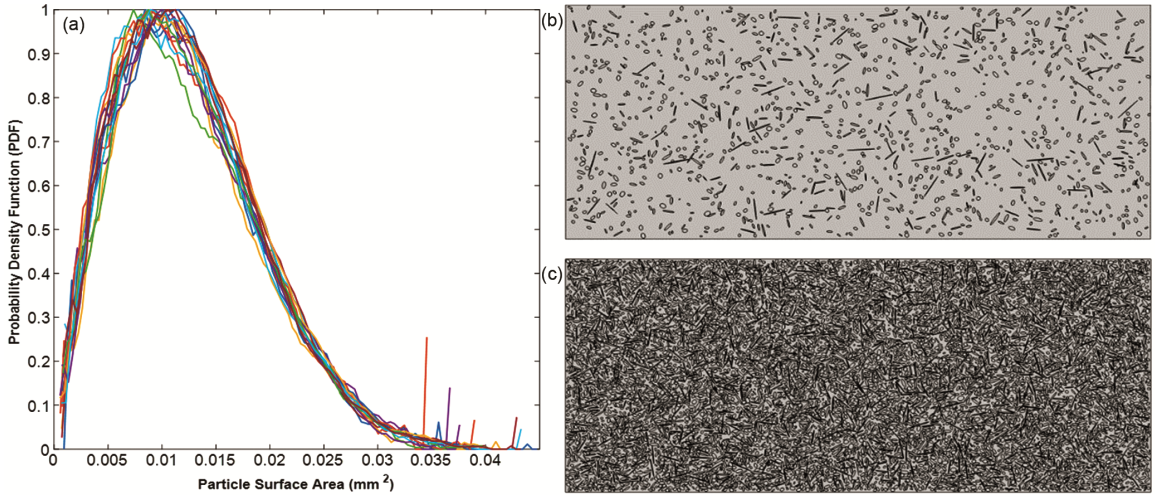

Fig. 14 — R-$(RC)_1$: (a) Rayleigh distribution of the samples, (b) Sample N° 1 (S=0.50), (c) Sample N° 13 (S=0.396)

number of inclusions with a high variability in particle sizes. This situation can have a significant impact on interfacial polarization, and consequently on the permittivity of the composite. For instance, for ε_i = 3600 and S = 0.39, we find that ε = 6.8 for the LN-RC_2, 7.2 for LN-RC_1, and 8.9 for LN-RC_3

3.1.3 Rayleigh Distribution (R)

The Rayleigh distribution is a common distribution used to model particle size. This distribution is characterized by a slow exponential decay of the Probability Density Function (PDF) as particle size increases (Figs. 14-16 (a)). Because of this slower decay, the Rayleigh distribution is able to generate a wider range of particle sizes than the Log-normal distribution.

The simulation results obtained with the Rayleigh distribution model of three series of samples (R-$(RC)_1$, R-$(RC)_2$, and R-$(RC)_3$) are summarized in Table 3.

It is remarkable that, in the context of the Rayleigh distribution, as the value of μ decreases, the number of inclusions increases. This trend is consistent with what we have observed in previous distributions. However, one significant achievement stands out here, demonstrating the effectiveness of the Rayleigh distribution in generating large numbers of particles. Taking the example of sample *N°* 13 in Table. 3 with a surface fraction of 0.39, we observed 7670 particles for R-$(RC)_1$ where μ =0.01mm^2 (represented in Fig. 14 (c)), 33372 particles for R-$(RC)_2$ with μ =0.03 mm^2 (Fig. 15.c), and 76907 particles for R-RC_3 with μ=0.001mm^2 (Fig. 16.c)

In Fig. 17, we plot the variation of the effective dielectric constant (ε) as a function of the size and surface fraction of the ellipsoidal particles for the three permittivities of particles ε_i=80 ,400, and 3600. several salient features can be observed. on the one hand, the results demonstrate that the permittivity (ε) of the composite is influenced both by the surface fraction (*S*) and by the permittivity and the size of the ellipsoidal inclusions. The graphs show that at low inclusion rates ranging from 0.05 to 0.12, the effective

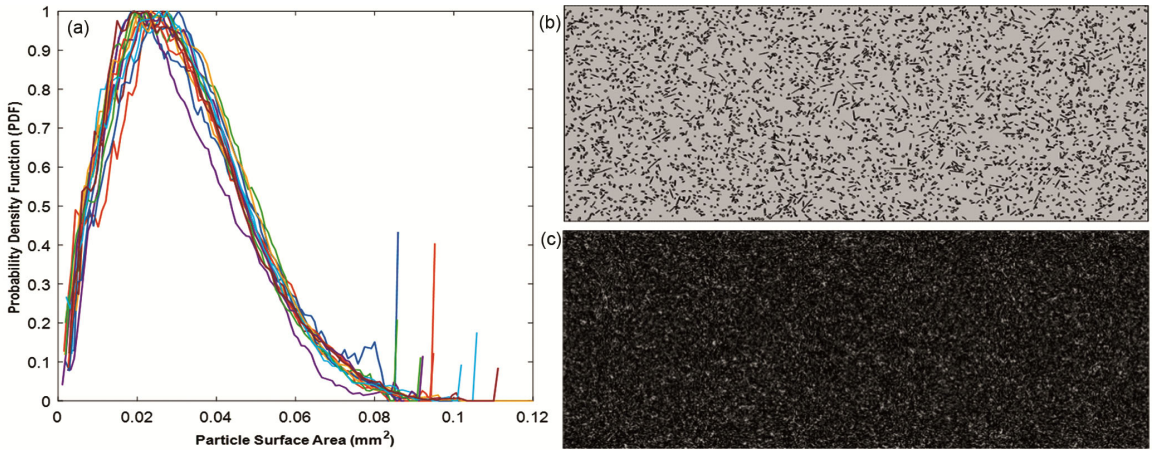

Fig. 15 — R-$(RC)_2$: (a) Rayleigh distribution of the samples, (b) Sample No 1 (S=0.55), (c) Sample N° 13 (S=0.399)

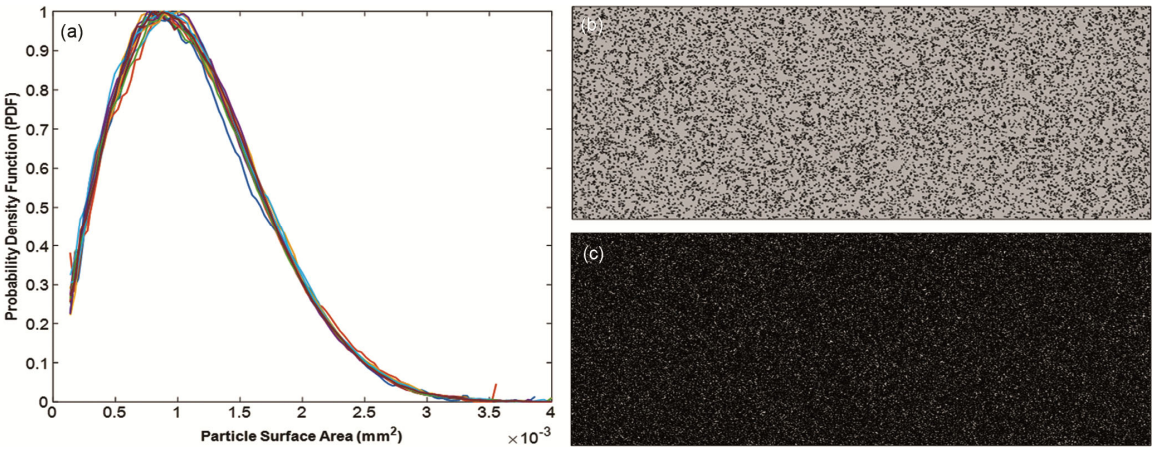

Fig. 16 — R-$(RC)_3$: (a) Rayleigh distribution of the samples, (b) Sample No 1 (S=0.50), (c) Sample N° 13 (S=0.396)

Table 3 — Characteristics of three series of RC composites simulated using the Rayleigh Distribution (R)

	R-$(RC)_1$		**R-$(RC)_2$**		**R-$(RC)_3$**	
	μ=0.01 mm² σ=0.006 mm²		μ=0.003 mm² σ=0.001 mm²		μ=0.001 mm² σ = 0.0006 mm²	
N^* Samples	N^0 *particles*	*S*	N^0 *particles*	*S*	N^0 *particles*	*S*
1	1198	0.050	4092	0.055	11908	0.050
2	1748	0.094	5881	0.080	15864	0.094
3	2290	0.127	8459	0.116	23776	0.127
4	2830	0.152	11244	0.153	31632	0.152
5	3384	0.181	13012	0.177	37485	0.181
6	3916	0.214	15791	0.213	43327	0.214
7	4447	0.241	18305	0.249	54816	0.241
8	4980	0.270	21673	0.296	54816	0.270
9	5497	0.298	23355	0.315	59619	0.298
10	5977	0.325	24937	0.335	64422	0.325
11	6296	0.355	26501	0.354	69225	0.355
12	7351	0.385	29334	0.376	73066	0.385
13	7670	0.396	33372	0.399	76907	0.396

permittivity ε shows minimal differences whatever the size and permittivity of the inclusions. However, beyond this range, as the surface fraction increases, a notable increase in effective permittivity is observed with divergence between the different simulated composites R-$(RC)_1$, R-$(RC)_2$, and R-$(RC)_3$. This

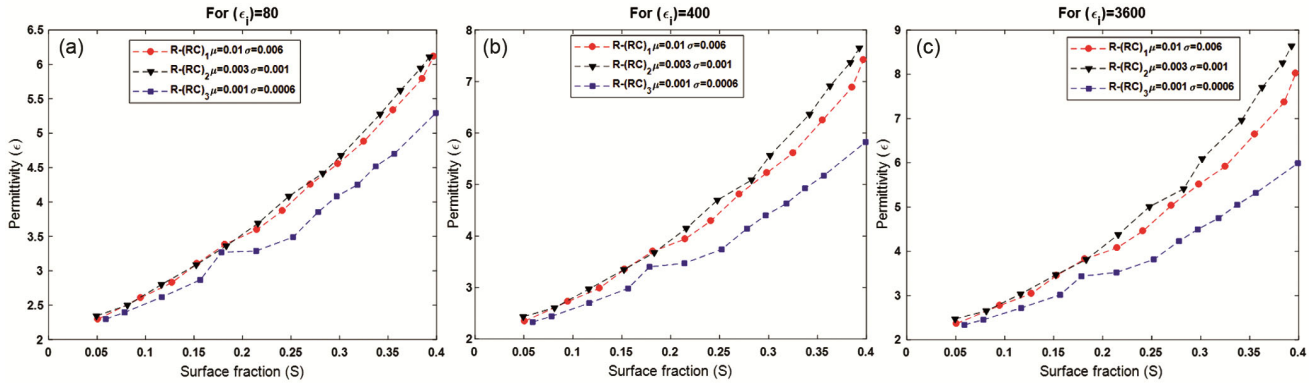

Fig. 17 — Evolution of the effective permittivity as a function of surface fraction for R-(RC) composites

divergence is more pronounced for inclusions with high permittivity (400 and 3600) due to its accentuated contrast with the matrix. The Rayleigh distribution model sensitivity to substantial changes in permittivity, together with intensified polarization effects, amplifies variations between simulated composites with different mean μ and standard deviation σ values. In particular, the R-$(RC)_2$ composite stands out with a higher permittivity than R-$(RC)_1$ and R-$(RC)_3$ because its inclusion size distribution provides superior balance. While R-$(RC)_1$ contains larger inclusions that may not interact effectively with the electric field due to their size, Conversely, in R-$(RC)_3$, the abundance of very small inclusions of very similar size, where the standard deviation is too small (σ =0.0006 mm^2) offers limited interaction with the electric field, leading to minimal impact on permittivity.

3.2 Simulated Results vs Theorical Models

Figures 18 and 19 show the correlation between the simulation results and the analytical models. The dielectric constant of the RC composites is plotted for each model as a function of the surface fraction of the ceramic filler particles. For the different distributions and particle sizes, the simulation results are presented alongside the theoretical predictions in each figure to examine the degree of agreement between them.

In order to quantify the average deviation between different values predict by models and the values found by simulation, a Root Mean Square Error (RMSE) was calculated by the following equation (Eq.13):

$$\mathrm{RMSE} = \sqrt{\frac{1}{N}\sum_{i=1}^{N}\left(\varepsilon_{exp} - \varepsilon_{model}\right)^2} \qquad \ldots(13)$$

Where N represents the number of samples, while ε_{exp} and ε_{model} represent the simulated and theorical permittivity, respectively.

3.2.1 Original Empirical Models

Figure 18 presents a comparison between the theoretical predictions of the original models and the corresponding simulation results. After careful examination of the graphs, it becomes apparent that models by Lichtenecker, Bruggeman, and Looyenga fail to accurately align with our simulated results. However, what is truly remarkable is the net advantage observed in the case of the Maxwell-Garnett (MG) model. This model displays a higher level of accuracy in its predictions, especially when dealing with RC composites with moderate inclusion permittivity (ε_i = 80). Nevertheless, as the permittivity of inclusions increases to levels of 400 and 3600, the disparities between our empirical results and theoretical projections derived from the Maxwell-Garnett model become more evident.

It is imperative to emphasize that the limitations inherent in the Maxwell-Garnett model appear in situations where interactions between particles become more complex due to high permittivity values with more pronounced particle concentration. it is remarkable in most graphs, when the surface fraction remains less than 0.15, the performance of the MG presents a certain degree of adequacy. Conversely, for surface fractions greater than 0.15, the MG equation does not correctly describe the simulated results, independently of the particle size and the type of distribution.

Table 4 lists the RMSE calculation between the dielectric constant predicted by the original mixing laws and the simulation results, for all cases of RC composites.

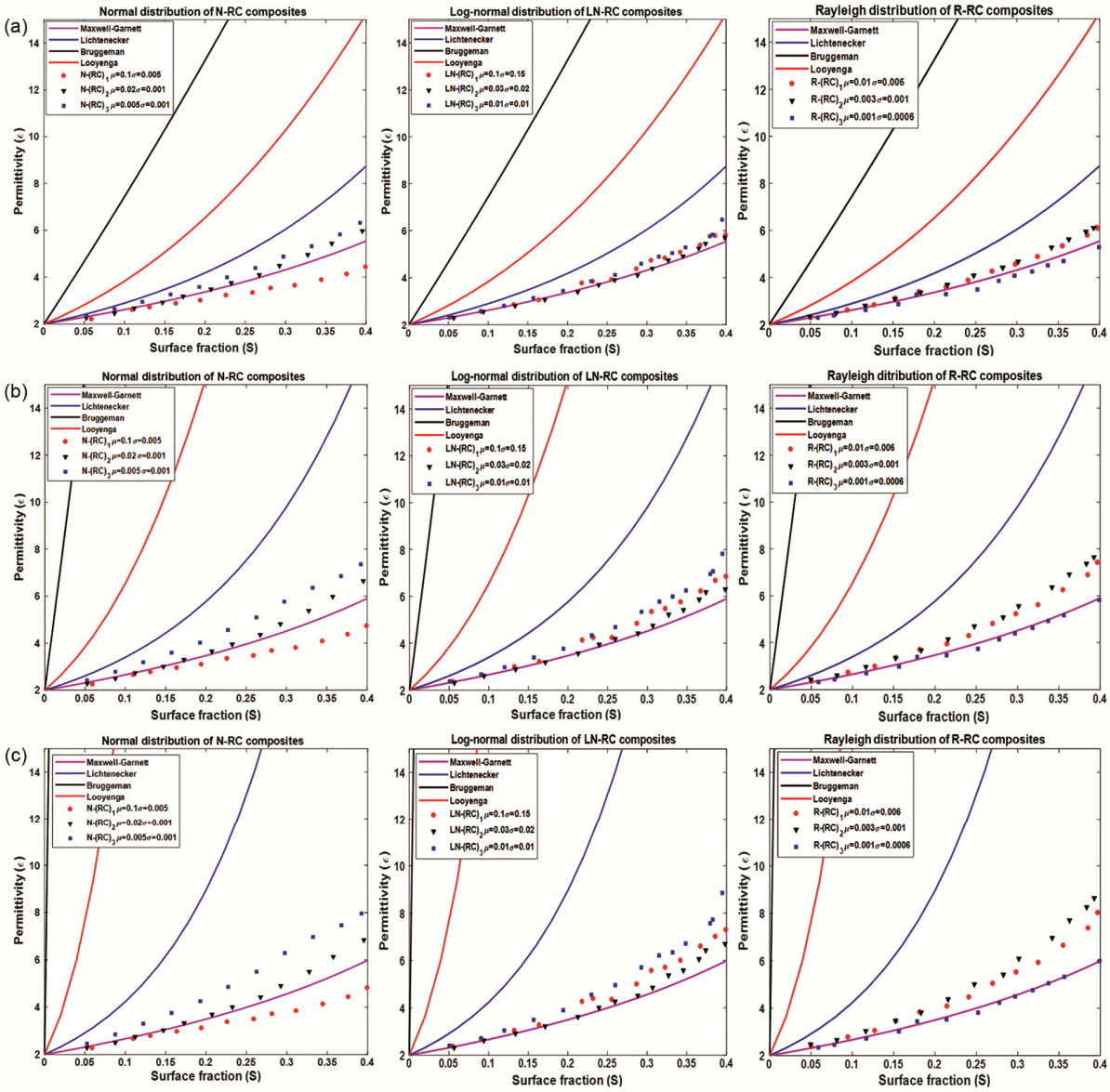

Fig. 18 — The effective permittivity modeling by original mixing laws for the different simulated RC composites

On the one hand, when $\varepsilon_i = 80$, we note that the error is smaller than 14 for every law in Table 4. this error becomes more important when the permittivity of the particles increases. Taking the case of N-$(RC)_1$ as an example, applying Lich's law, we find an RMSE= of 2.29 for ε_i=80, it becomes 5.98 for ε_i =400, then 16.43 for ε_i=3600. On the other hand, all results show that the Maxwell-Garnett model has the lowest error for all distributions. This could be due to the sensitivity of this model in predicting the effective properties of composites when the shape of the inclusions is close to spherical. It is noteworthy that this group of original laws does not effectively predict the dielectric constant because they do not have information about the size and distribution of the particles in the matrix.

3.2.2 Modified Empirical Models

The comparison between the modified theoretical models and the simulated results for the different dielectric composites is shown in Fig. 19. Obviously, these models show improved performance compared to the original laws. This improvement can be attributed to the incorporation of information on the shape and polarization of inclusions into these

Table 4 — Root Mean Square Error values of original mixture laws for the different simulated RC

	Models	Maxwell-Garnett	Lichtenecker	*Bruggeman*	*Looyenga*
RMSE for $\varepsilon_i = 80$	N-RC_1	0.6399	2.2967	13.8217	6.053
	N-RC_2	0.2355	1.293	12.1959	4.7817
	N-RC_3	0.4839	1.11	12.2737	4.7262
	LN-RC_1	0.2312	1.5782	13.7945	5.6132
	LN-RC_2	0.1105	1.7117	13.9626	5.7462
	LN-RC_3	0.3997	1.442	13.7049	5.5221
	R-RC_1	0.2786	1.408	13.0052	5.2042
	R-RC_2	0.3671	1.3511	13.0724	5.214
	R-RC_3	0.2003	1.7829	13.1908	5.4648
RMSE for ε_i =400	N-RC_1	0.6751	5,9812	75,7035	24,2876
	N-RC_2	0,3778	4,445	70,0941	21,2408
	N-RC_3	0,9915	4.1102	71,5216	21.6725
	LN-RC_1	0,5855	5,18	79,1841	24,9691
	LN-RC_2	0,2891	5,4281	79,5433	25,132
	LN-RC_3	0,9748	4,8931	79,2298	24,9848
	R-RC_1	0,7382	4,6625	74,7894	23,2108
	R-RC_2	1,0167	4,4931	75,4467	23,4257
	R-RC_3	0,1115	5,1562	73,995	5.4648
RMSE for ε_i =3600	N-RC_1	0,6808	16,4342	695,9904	159,6589
	N-RC_2	0,4255	13,7069	652,0291	143,6422
	N-RC_3	1,3448	13,679	670,4512	150,6533
	LN-RC_1	0,7587	16,3582	738,379	171,8925
	LN-RC_2	0,3903	16,4427	739,0499	170,6463
	LN-RC_3	1,3611	16,1096	741,84	174,659
	R-RC_1	0,9765	15,0867	698,7134	160,6552
	R-RC_2	1,4737	14,9055	706,9592	163,7853
	R-RC_3	0,0878	14,9197	684,7853	152,5478

models, highlighting their importance in predicting composite dielectric permittivity.

More precisely, when examining the graphs for ε_i =80, we observe that the models of Maxwell-Garnett, Yamada project with greater precision than those of Bruggeman and Bergman, in particular for surface fractions of charge greater than 0.2.

To go further, the models of Maxwell Garnett, Yamada were selectively applied to scenarios of high inclusion permittivities (ε_i = 400 and ε_i = 3600). This research aimed to understand the variable influence of factors related to shape and depolarization.

Looking at the Maxwell-Garnett and Yamada models, the Maxwell-Garnett depolarization factor (A) and Yamada shape parameter (n) show limited variation with increased inclusion permittivity. More specifically, Maxwell Garnett's depolarization factor (A) is a parameter that measures the capacity of a material to polarize in response to an applied electric field. Lower A values indicate a high polarizability of the inclusions, this can lead to an improved effective permittivity of the composite material. Considering the case of the normal distribution of RC composites for ε_i =400 in Fig 19.b. it is clear that N-$(RC)_3$, which gives the best permittivity, has a lower A factor of 0.23 compared to N-$(RC)_1$ and N-$(RC)_2$, which have factors of 0.47 and 0.28, respectively.

Furthermore, in the context of the Yamada model, taking the same example, we observe a transition from n = 2.1 for N-$(RC)_1$ to n = 4.4 for N-$(RC)_3$. An n value of 2.1 implies relatively rounded but not spherical ellipsoidal inclusions, while n = 4.4 suggests elongated inclusions. This increased elongation corresponds to a stronger alignment of the inclusions with the electric field, potentially contributing to distinct electrical responses within the composite.

Table 5 summarizes the RMSE found, determined by Eq. (13), between theoretical and simulated results for the modified mixing laws. we can see that the modified Yamada and Maxwell Garnett models give the best fit to the simulated results compared to Bruggeman and Bergman with an error value less than 0.2.

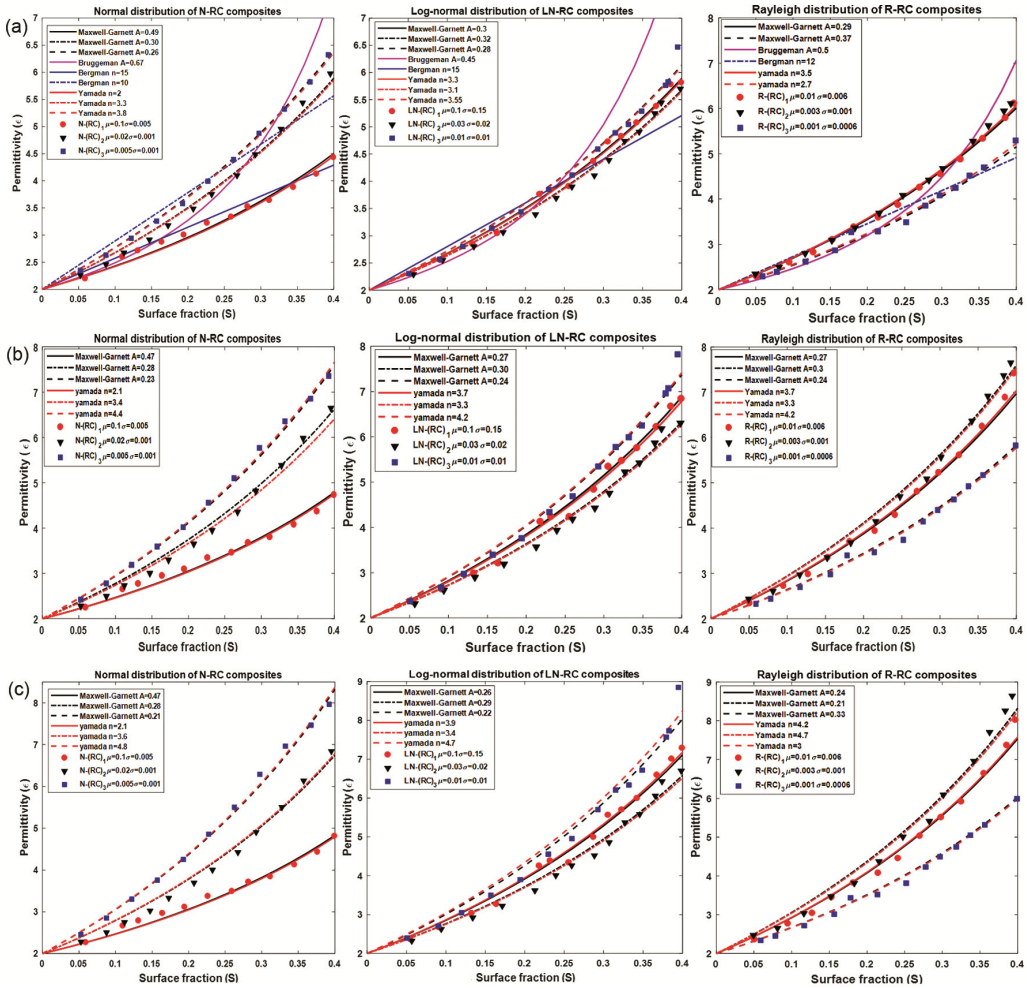

Fig. 19 — The effective permittivity modeling by modified mixing laws for the different simulated RC composites

Table 5 — Root Mean Square Error values of modified mixture laws for the different simulated RC composites.

	Models	Modified MG	Modified *Bruggeman*	*Bergman*	*Yamada*
RMSE for $\varepsilon_i = 80$	N-RC$_1$	0.0956	1.7969	0.0999	0.0943
	N-RC$_2$	0.1061	0.8175	0.3095	0.1113
	N-RC$_3$	0.0343	1.8564	0.2560	0.0376
	LN-RC$_1$	0.0802	1.1034	0.8827	0.0827
	LN-RC$_2$	0.0935	1.1590	0.7364	0.0914
	LN-RC$_3$	0.1298	0.9555	1.0674	0.1309
	R-RC$_1$	0.0678	1.0027	0.2771	0.0771
	R-RC$_2$	0.1032	0.9008	0.3028	0.0805
	R-RC$_3$	0.0821	1.5050	0.2102	0.0820
RMSE for ε_i =400	N-RC$_1$	0.1014	-	-	0.0994
	N-RC$_2$	0.1478	-	-	0.1616
	N-RC$_3$	0.0904	-	-	0.0811
	LN-RC$_1$	0.1225	-	-	0.1230
	LN-RC$_2$	0.1431	-	-	0.1436
	LN-RC$_3$	0.1820	-	-	0.1786
	R-RC$_1$	0,1693	-	-	0,1495
	R-RC$_2$	0.1552	-	-	0.1582
	R-RC$_3$	0,0879	-	-	0,081

(*Contd.*)

Table 5 — Root Mean Square Error values of modified mixture laws for the different simulated RC composites.

	Models	Modified MG	Modified *Bruggeman*	*Bergman*	*Yamada*
RMSE for ε_i =3600	N-RC_1	0.1008	-	-	0.1023
	N-RC_2	0.1559	-	-	0.1586
	N-RC_3	0.1312	-	-	0.1259
	LN-RC_1	0.1548	-	-	0.1468
	LN-RC_2	0.1746	-	-	0.1746
	LN-RC_3	0.2957	-	-	0.3024
	R-RC_1	0,19	-	-	0,184
	R-RC_2	0,2627	-	-	0,279
	R-RC_3	0,0983	-	-	0,0878

4 Conclusion

In this article, we studied binary epoxy resin/ceramics (RC) composite materials through a series of 2D simulations using the finite element method (FEM) under quasistatic conditions. A new algorithm was developed and implemented in MATLAB to generate random distributions of ellipsoidal ceramic particles within the epoxy resin polymer matrix which has dimensions of a WR90 rectangular waveguide.

This work aimed to conduct a thorough examination of the impact of permittivity, concentration, distribution and particle size on the dielectric behavior of the RC composite on the one hand, and to meeting the challenge to simulate a significant number of ceramic particles distributed in the matrix on the other hand.

Divided into two distinct parts, in the first one, the research effort focused on the study of three distribution models (Normal, Log-normal, and Rayleigh) to describe the distribution of surface particles at the matrix level. For each distribution model, three cases of particle sizes were examined and applied on three RC composites with an inclusion permittivity of 80, 400, and 3600 leaving the permittivity of the matrix fixed. Notably, in all models, the results showed that the effective permittivity of all RC composites increases when the permittivity and the surface fraction of the particles also increase. Furthermore, the results show the major impact of particle size and distribution on the interfacial interactions in the material, where it was observed that composites that contain a diversity of particle sizes introduce an obvious effect on the overall permittivity of composite. In addition, the Rayleigh distribution demonstrated exceptional efficiency in allowing the successful simulation of more than 70,000 non overlap ellipsoidal particles distributed in the rectangular matrix, which is not the case for the Normal and Log-normal distributions.

In the second part, theoretical "mixing laws" models were applied to predict the dielectric permittivity of our RC materials, stratified into two categories. The first category includes classical models with spherical inclusions dispersed in a continuous matrix. In contrast, the second category contains modified laws that introduce information about the shape and depolarization factors of particles. Through a systematic analysis of these models with our different simulated results, it becomes evident that the modified models more accurately predict the dielectric behavior of composites. it was found that the modified models of Maxwell-Garnett and Yamada turned out to be exceptionally accurate. where it was observed that these models agree with the simulated results with an error lower than 0.2.

The implications of this research are of considerable importance, as they contribute to the development of new optimized materials (such as phase shifters, filters, and various microwave devices) through a comprehensive analysis of their electromagnetic properties before their production using detailed simulations. Future work may exploit optimization methods such as Artificial Intelligence to achieve satisfactory particle distribution within the matrix with optimal prediction of material behavior, and extend research to the frequency domain, thus opening up new research and application perspectives.

References

1 Ngo T D, Intechopen*, Alberta Innovates, Canada*, (2020).
2 Hull D & Clyne T W, *Cambridge University Press, Cambridge*, (1996).
3 Delfouf R, Bouzit N, Bourouba N, Martinez Jimenez J P, Brahimi A, Khouni H & Arab T, *ECS J Solid State Sci Technol*, 11 (2022) 073006.
4 Khouni H, Bouzit N, Jiménez J P M & Bouamar M, *Eur Phys J Appl Phys*, 76 (2016).
5 Balasubramanian M, Composite Materials and Processing, *CRC Press*, Boca Raton, (2013).
6 Djouada D, Bouzit N, Delfouf R, Chioukh L & Jiménez J P M, *ECS J Solid State Sci Technol*, 12 (2023) 063003.
7 Lee H & Kim H, *J Appl Phys*, 67 (1990) 2024.

8 Araújo M C, Costa C M & Lanceros-Méndez S, *J Non-Cryst Solids*, 387 (2014) 6.
9 Aboubakr S, Hajjaji A, Rguiti M, Benkhouja K, Courtois C & Boughaleb Y, *Eur Phys J Appl Phys*, 81 (2018) 2.
10 Kamar E M, Khairy M & Mousa M A*, J Mater Res Technol*, 24 (2023) 7381.
11 Brosseau C, *J Phys D*, 39 (2006) 1277.
12 Torquato S, *Springer, New York*, (2002).
13 Zhang Z et al, Polymers, 16 (2024) 4.
14 Lu X et al, *Compos Sci Technol*, 194 (2020).
15 Brosseau C & Beroual A, *Prog Mater Sci*, 48 (2003) 373.
16 Jebbor N & Bri S, *J Electrostat*, 70 (2012) 393.
17 Sareni B, Krähenbühl L, Beroual A & Brosseau C, *J Appl Phys*, 81 (1997) 2375.
18 Dale G, Strawhorne M, Sinclair D C & Dean J S, *J Am Ceram Soc*, 101 (2018) 1211.
19 Pérez-Higareda J R et al, *Model Simul Mater Sci Eng*, 32 (2024) 1.
20 Delfouf R, Bouzit N, Bourouba N, Brahimi A & Jiménez J P M, *ECS J Solid State Sci Technol*, 11 (2022) 093003.
21 Brahimi A, Bourouba N, Martinez Jiménez J P & Bouzit N, *J Compos Adv Mater*, 31 (2021) 181.
22 Arab T *et al., ECS J Solid State Sci Technol,* 12 (2023) 043005.
23 Khouni H, Thèse de Doctorat, Université Mohamed Boudiaf de Msila, (2017).
24 Benhamouda A, Thèse de Doctorat, Université Ferhat Abbas, Sétif, (2018).
25 Jebbor N & Bri S, *J Electrostat*, 70 (2012) 393.
26 Kaufman J L *et al*., *AIP Adv*, 8 (2018) 125020.
27 Zhong S L, Dang Z M & Zha J W, *IEEE Trans Dielectr Electr Insul*, 25 (2018) 2122.
28 Oussef O, Seddik B, Chrif B & Mohamed H, FME *Trans*, 48 (2020) 908.
29 COMSOL AB, COMSOL Multiphysics Reference Manual, Stockholm, Sweden.
30 Jebbor N, Thèse de Doctorat, Université Moulay Ismail, Maroc, (2014).
31 Mejdoubi A, Thèse de Doctorat, Université de Bretagne Occidentale, France, (2007).
32 Eberly D, Intersection of Ellipses, Geometric Tools, Redmond WA 98052, (2020).
33 COMSOL, *LiveLink MATLAB Guide,* LiveLink Guide for COMSOL Multiphysics, Version 5.6, COMSOL Inc., (2021).
34 Choy T C, *Effective Medium Theory: Principles and Applications,* 2nd edn, (2015).
35 Chi Q G, Dong J F, Zang C H, Wong C P, Wang X & Lei Q Q, *J Mater Chem C*, 35 (2016) 8179.
36 Qi F, Chen N & Wang Q, *Mater Des*, 131 (2017) 135.
37 Araújo M C, Costa C M & Lanceros-Méndez S, *J Non-Cryst Solids*, 387 (2014) 6.
38 Looyenga H, *Physica*, 31 (1965) 401.
39 Mejdoubi A & Brosseau C, *J Appl Phys*, 99 (2006) 063502.
40 Bergman D J, *Phys Rep*, 43 (1978) 377.
41 Yamada T, Ueda T & Kitayama T, *J Appl Phys*, 53 (1982) 4328.
42 Chelghoum R, *et al.*, *ECS J Solid State Sci Technol*, 13 (2024) 043018.